Quantum thermalization in a dimerized $J_1 - J_2$ model

Smitarani Mishra and Shaon Sahoo* Department of Physics, Indian Institute of Technology, Tirupati

We revisit the $J_1 - J_2$ frustrated Heisenberg spin-1/2 chain with dimerization (δ) or modulation in the nearest-neighbor couplings to investigate its thermalization behavior. While the dimerization tends to induce localization, the next-nearest-neighbor interaction J_2 generally favors thermalization, making the assessment of the model's compliance with the Eigenstate Thermalization Hypothesis (ETH) particularly subtle. The challenge is further compounded by the model's SU(2) symmetry; the study of ETH compliance is necessarily done for each symmetry sector but separating different sectors of this symmetry is known to be a computationally demanding task. The current study is driven by two main motivations: first, to explore whether the well-known ground-state phases of the model have any bearing on its thermalization properties; and second, to understand how the interplay between two competing factors, namely, the non-uniformity (via δ) and the beyond-nearestneighbor interactions (via J_2) governs the system's approach to thermal equilibrium. A systematic analysis shows that the ETH is most strongly satisfied for intermediate values of δ (~ 0.5) with J_2 ranging from intermediate (~ 0.5) to large (~ 1) - a parameter regime falls within the spiral ground-state phase. It is also found that when the system is in the gapless ground-state phase (which falls within the Néel phase), the ETH is more prone to violation. In the regime of large δ and small J_2 , the system is seen to enter a localized phase (characterized here by modulation in density-of-states); assessing ETH compliance is less meaningful for this phase.

I. INTRODUCTION

The thermalization of isolated quantum systems remains a central challenge in contemporary theoretical physics, shaped by the complex interplay of quantum coherence, entanglement, and interactions. The Eigenstate Thermalization Hypothesis (ETH) has become a key framework for understanding how closed quantum systems thermalize [1–5]. The ETH has been extensively supported through studies in a variety of settings, including standard spin models [5–9], disordered spin chains [10], and models with long-range interactions [11, 12]. However, the ETH breaks down in integrable systems [13–16] and many-body localized (MBL) phases [17–20], where usual (Gibbsian) thermalization fails. Its validity has been further examined in disordered Hubbard models [21], and quantum breakdown scenarios [22]. Recent experimental advances with programmable quantum simulators [23–25] have directly tested ETH predictions, reinforcing its foundational role in quantum statistical mechanics.

The thermalization in clean one-dimensional spin chains is relatively well understood [4, 5, 26, 27]. The presence of disorder, inhomogeneity, or long-range interactions introduces new complexity [11, 15, 28–33]. For example, long-range interactions can be shown to be responsible for phenomena such as prethermalization [31] and disorder or inhomogeneity may give rise to many-body localization (MBL) and ergodicity breaking (violation of ETH) [15, 34]. The dimerized $J_1 - J_2$ Heisenberg spin-1/2 chain is a well-known model with a rich ground-

state phase diagram [35]. This model offers a minimal yet nontrivial setting to study thermalization under both inhomogeneity (via dimerization δ in the nearest-neighbor couplings) and extended-range interactions (via the next nearest-neighbor couplings J_2). This, in fact, is a key motivation behind our investigation of the thermalization properties of this model. The other motivation for our current study is to investigate whether the well-known ground-state phases of the model have any connection to its mid-spectrum thermalization behavior.

To study the thermalization behavior of the spin model and assess the extent to which the ETH is obeyed, we primarily compute the nearest-neighbor spin-spin correlation function $\langle S_1^z S_2^z \rangle$ across all eigenstates of the model. The mid-spectrum fluctuation σ_{sc} of this function provides a quantitative measure of ETH compliance, with smaller values indicating stronger adherence. To better understand the thermalization property of the model, we also calculate the effective dimension of subsystem d_{eff} (a convenient measure of entanglement entropy) and the average von Neumann (VN) entropy \overline{S}_{vn} over all eigenstates. Our main findings are summarized as follows. (1) When the system has a gapless ground-state phase, the ETH is more prone to violation. (2) In general, the ETH holds more strongly when the system has the gapped spiral phase compared to when it has the gapped Néel phase. (3) In the regime of large dimerization (δ) and small nextnearest-neighbor coupling (J_2) , the system enters in to a localization phase; here the energy spectrum exhibits a banded structure with gaps (revealed as a modulation in the density-of-states, DOS). (4) In general, the entanglement entropy across the energy spectrum displays multiple branches due to SU(2) symmetry and localization (connected to the modulation in DOS).

^{*} Corresponding author: shaon@iittp.ac.in

The paper is organized as follows. We discuss the J_1-J_2 model with dimerization in Sec. II, followed by a discussion on its ground-state phase diagram in Sec. III. Next, in Sec. IV, we discuss in detail the thermalization behavior of the model in the $\delta-J_2$ parameter space. We conclude our work in Sec. V.

II. MODEL

The $J_1 - J_2$ Heisenberg spin-1/2 chain with dimerization (staggered nearest-neighbor interactions) [36, 37] serves as a prototypical model for studying quantum magnetism with frustration. Its Hamiltonian is given by:

$$H = J_1 \sum_{i=1}^{N} \left[1 + (-1)^i \delta \right] \mathbf{S}_i \cdot \mathbf{S}_{i+1} + J_2 \sum_{i=1}^{N} \mathbf{S}_i \cdot \mathbf{S}_{i+2}, (1)$$

where $\mathbf{S}_i = (S_i^x, S_i^y, S_i^z)$ represents the spin-1/2 (vector) operator at the site i, N is the total number of sites, and δ is the dimerization strength. The parameter J_2 represents the next-nearest-neighbor exchange coupling, which is responsible for inducing frustration in the system. We take $J_1 = 1$ for this work. The term $[1 + (-1)^i \delta]$ introduces a spatial modulation in the nearest-neighbor interactions, leading to a staggered pattern of coupling strengths. The periodic boundary conditions are assumed, such that $\mathbf{S}_{N+1} = \mathbf{S}_1$ and $\mathbf{S}_{N+2} = \mathbf{S}_2$. The periodic boundary conditions are crucial for avoiding edge effects in finite systems and have been extensively used in numerical studies of one-dimensional quantum magnets [38]. A schematic diagram of the model is presented in Fig. 1.

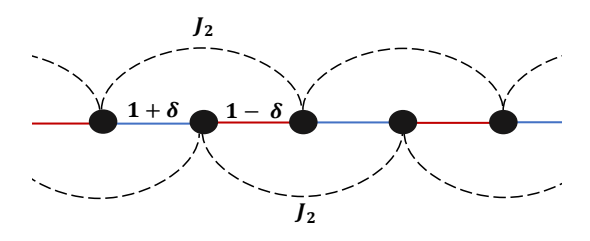


FIG. 1: Schematic representation of the $J_1 - J_2$ Heisenberg spin chain with dimerization (δ) in the nearest-neighbor interactions (J_1). Each filled circle represents one spin.

When $J_2=0$ and $\delta=0$, the model reduces to a standard nearest-neighbor Heisenberg spin chain. As J_2 increases, the competition between the nearest-neighbor and next-nearest-neighbor interactions leads to different ground-state phases. A particularly interesting case arises when $J_2=0.5$ and $\delta=0$, which corresponds to the Majumdar-Ghosh model [36]. In this case, the Hamiltonian becomes:

$$H_{\text{MG}} = \sum_{i=1}^{N} \mathbf{S}_i \cdot \mathbf{S}_{i+1} + 0.5 \sum_{i=1}^{N} \mathbf{S}_i \cdot \mathbf{S}_{i+2}.$$
 (2)

The ground-state of the Majumdar-Ghosh model can be found exactly; the ground-state is found to be doubly degenerate, consisting of dimerized spin-singlet pairs. This model provides a key example of frustration in one-dimensional spin systems and has been extensively studied in the context of quantum phase transitions and entanglement properties [36, 39, 40].

Inclusion of the dimerization term δ further enriches the behavior of the system. The ground-state phase diagram in the $\delta - J_2$ plane is discussed in the next section.

III. GROUND-STATE PHASE DIAGRAM

In this section, we briefly discuss the ground-state phase diagram of the model [35], which is schematically shown in Fig. 2.

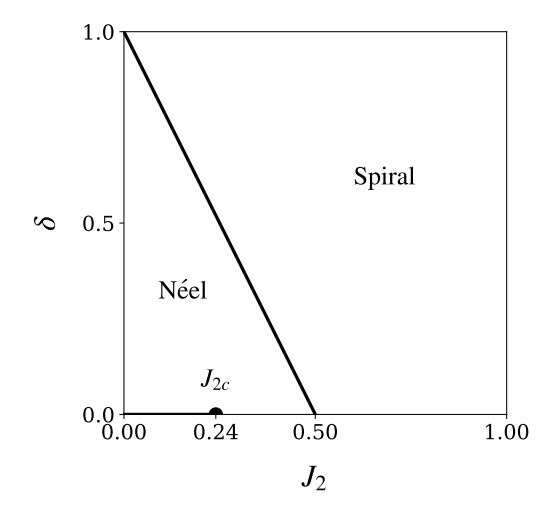


FIG. 2: Schematic ground-state phase diagram of the J_1-J_2 spin-1/2 chain with dimerization (δ) . The model exhibit two phases - Néel and Spiral - separated by the straight line $2J_2+\delta=1$. Along this line, product of dimers represents the exact ground-state. The whole diagram corresponds to gapped phases, except on the line segment $0 \le J_2 \le J_{2c} \approx 0.241$ with $\delta=0$ where the system is gapless.

The uniform chain $(\delta=0)$ without frustration $(J_2=0)$ is just the Haldane spin-1/2 chain which is known to have gapless ground-state [41]. The uniform chain remains gapless with the frustration strength up to $J_2 \leq J_{2c} \approx 0.241$, beyond which $(J_2 > J_{2c})$, the system becomes gapped [37]. The system goes through a quantum phase transition at $J_2 = J_{2c}$. In the phase diagram, $J_2 = 0.5$ represents a special point where the product of the nearest-neighbor dimers represents the exact ground-state of the model (it is also two-fold degenerate) [36].

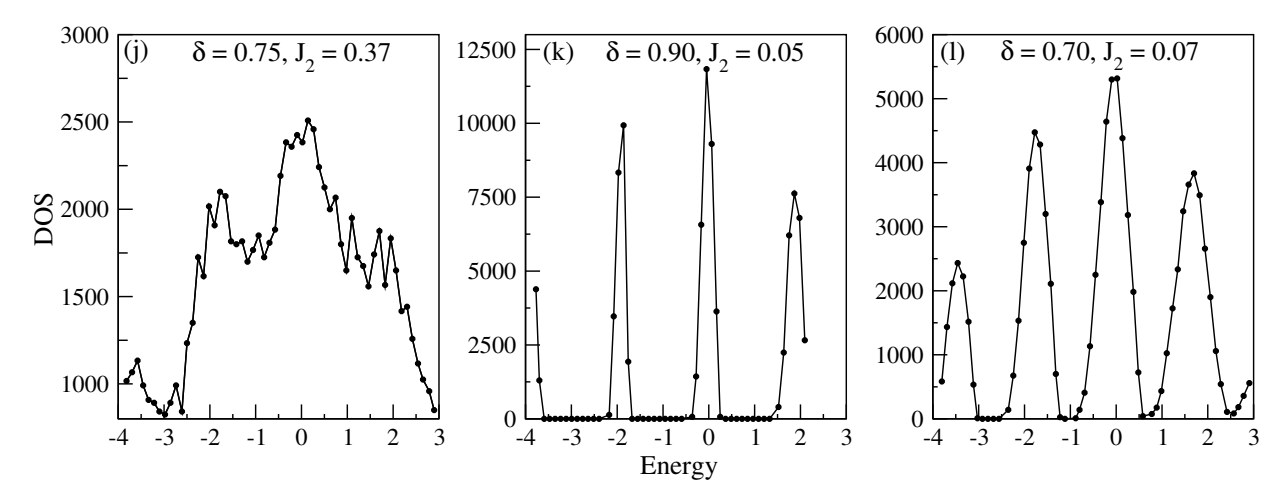


FIG. 3: Density of states (DOS) profiles across the energy spectrum for the three selected points (j) - (l) (see Fig. 4).

With dimerization $\delta > 0$, the ground-state phase becomes gapped [35]. In fact, the whole ground-state phase diagram is gapped except when $\delta = 0$ and $0 \le J_2 \le J_{2c}$. The phase diagram shows a crossover (disorder) line, $2J_2 + \delta = 1$; to the left side of this line, the system shows a Néeel phase, whereas, to the right side of the line, the system shows a spiral phase. In the phase diagram, another interesting line is $\delta = 1$; this line corresponds to a ladder system (two coupled chains) for any finite value of J_2 .

IV. THERMALIZATION PROPERTIES

In the previous section, we outlined the ground-state phases of the dimerized J_1 - J_2 spin- $\frac{1}{2}$ chain. We now turn to a systematic study of the model's thermalization behavior. Our analysis is based on exact diagonalization performed within the $S_z=0$ sector, where S_z denotes the z-component of the total spin. Although the model possesses SU(2) symmetry - implying that the $S_z=0$ sector can be further decomposed into subspaces with definite total spin S - numerically resolving these finer sectors becomes increasingly difficult as system size grows [42, 43]. Therefore, we restrict our computations to the full $S_z=0$ sector

An important consequence of not fully resolving all symmetry sectors is the emergence of multiple branches in plots of the entanglement entropy across the many-body energy spectrum. We return to this point and discuss it in detail later.

A. Local observable and mid-spectrum fluctuation

Quantum thermalization refers to the process by which, after a long time of evolution, the expectation value of a local observable matches what is predicted by

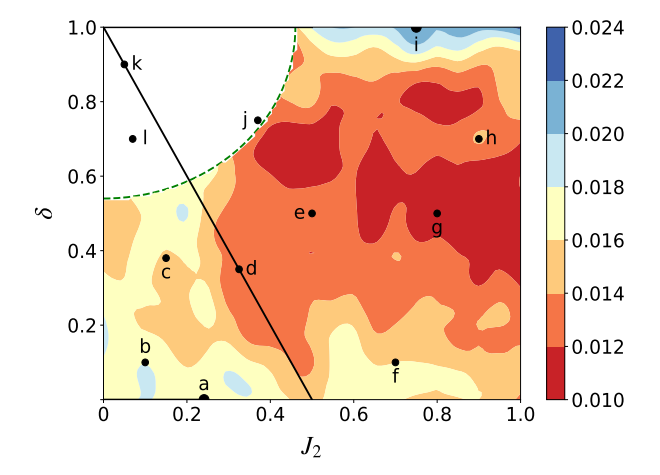


FIG. 4: Thermal phase diagram of the J_1-J_2 model with dimerization. It shows the value of mid-spectrum fluctuation σ_{sc} of a local observable. The disorder line, $2J_2+\delta=1$, is shown on the diagram. The fluctuation is not calculated in the white region which is separated by a dotted line encircling the point $(\delta=1,J_2=0)$. The points mentioned on the diagram, (a) - (l), are separately studied in detail.

the microcanonical ensemble. This requires that, within a narrow energy window, the expectation values of the observable in different eigenstates be nearly identical. This forms the basis of the Eigenstate Thermalization Hypothesis (ETH), which is typically satisfied in nonintegrable systems [1, 2, 4, 5].

The above discussion highlights that fluctuations in the expectation values of a local observable corresponding to eigenstates associated with a narrow energy window serve as a key indicator of ETH compliance — smaller fluctuations imply stronger thermalization and closer adherence to the hypothesis. We take the following operator as the local observable: $O = S_1^z S_2^z$. The

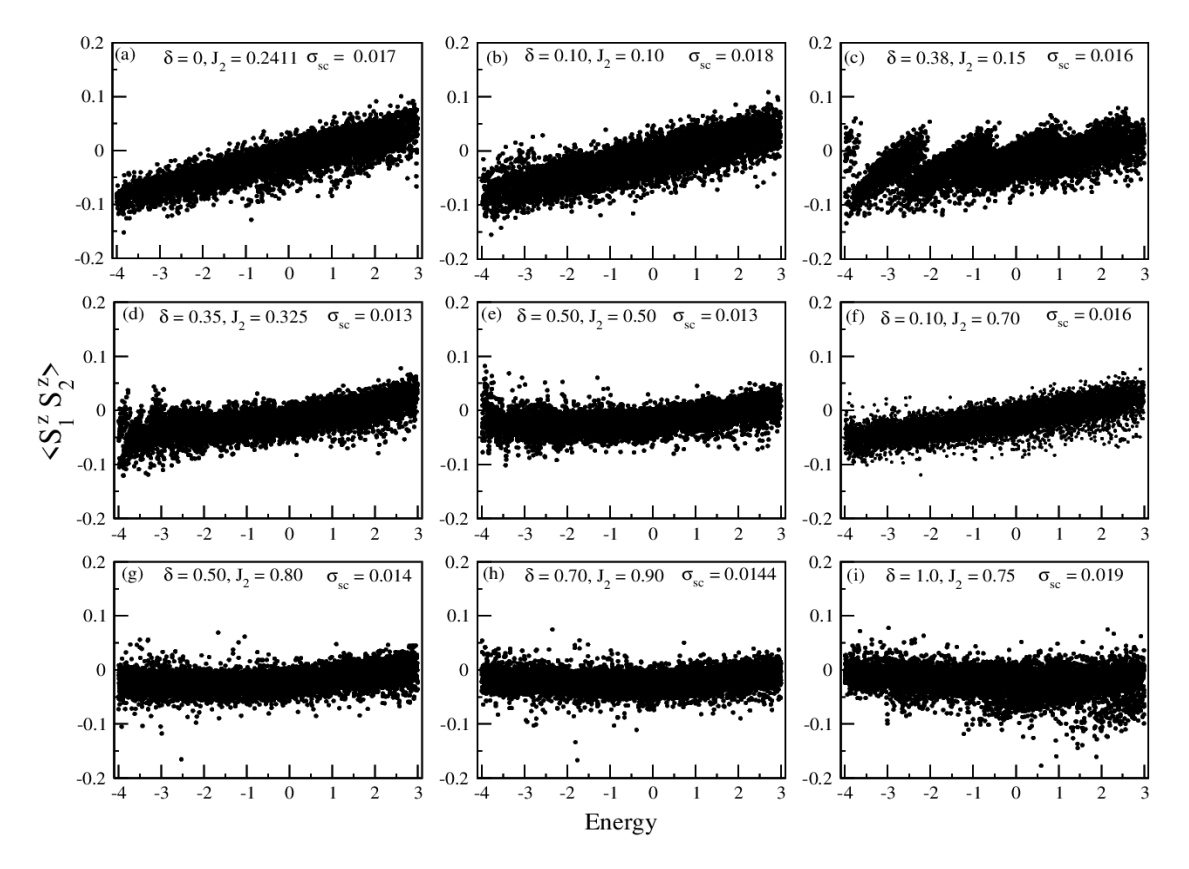


FIG. 5: Expectation value of the local operator for individual eigenstates, $\langle S_1^z S_2^z \rangle$, is plotted across the energy spectrum. Plots are shown for the points (a) - (i) from Fig. 4.

expectation value of O gives the nearest-neighbor spinspin corelation. In the middle of the spectrum (where the density of states is largest), we calculate the fluctuation of the observable in the following way:

$$\sigma_{sc} = \sqrt{\overline{O^2} - \overline{O}^2}. (3)$$

Here \overline{O} is the expectation value averaged over different eigenstates, i.e., $\overline{O} = \frac{1}{D} \sum_{i=1}^{D} \langle i | O | i \rangle$, where the eigenkets $|i\rangle$ are from the narrow energy window and there are D eigenkets in the window. We can also define $\overline{O^2}$ similarly.

For system size N=16 and subsystem size $N_s=6$, we calculate σ_{sc} across the parameter space $0 \le \delta \le 1$ and $0 \le J_2 \le 1$, except for a region in the top-left corner of the thermal phase diagram (see Fig. 4). In this white region, the energy spectrum exhibits a banded structure with gaps, as is evident from the density of states (DOS) plots in Fig. 3. It is not difficult to see why the spectrum behaves this way. When $\delta=1$, the system becomes a ladder; here J_2 is the exchange constant along the two legs and $J_1=2$ is the exchange constant along the rungs. Now, when $J_2=0$, we get disconnected rungs. For the collection of disconnected rungs, the spectrum is a set of discrete energies (with degeneracies). As J_2 increases, we get a band-like structure that is observed in

Fig. 3. In this regime (large δ and small J_2), the system is evidently in a localized phase since it corresponds to weakly interacting dimmers (rungs).

Our numerical results presented in Fig. 4 show that the ETH holds more robustly when the value of δ is intermediate (~ 0.5) and the value of J_2 is in the range between intermediate (~ 0.5) and large (~ 1). In this regime, the fluctuation of the local observable σ_{sc} is small, and this region falls within the spiral ground-state phase mentioned earlier. It is interesting to note that, although dimerization induces localization, a delicate balance between finite δ and J_2 here helps the system to thermalize strongly according to the ETH.

For better understanding of the thermalization of the model and the degree of the ETH compliance, for some specific points from Fig. 4, we plot the expectation values of the local operator $O=S_1^zS_2^z$ for different eigenstates across the energy spectrum. The results are presented in Fig. 5.

B. Effective dimension of subsystem

To gain more insight into the thermalization properties of the $J_1 - J_2$ model with dimerization, we now

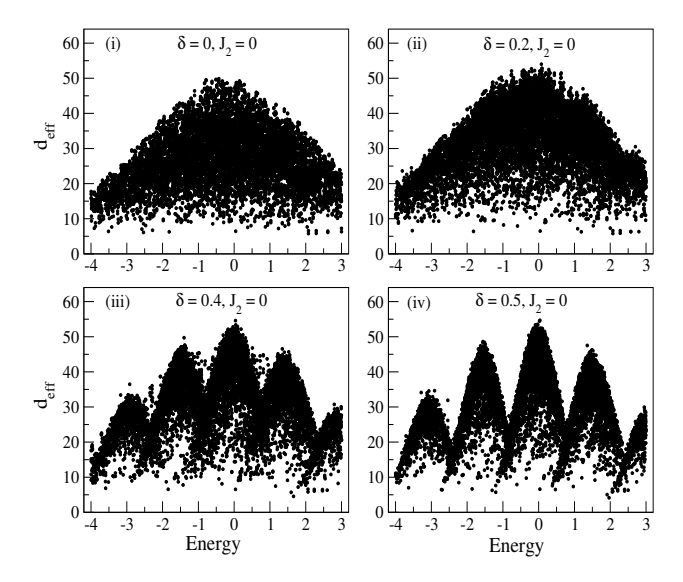


FIG. 6: Effective dimension d_{eff} of the subsystem for the individual eigenstates across the energy spectrum is shown for some δ values (with $J_2 = 0$).

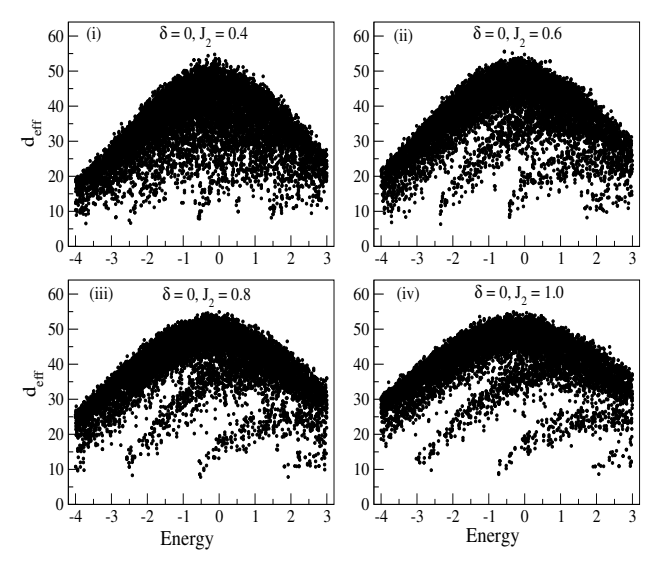


FIG. 7: Effective dimension d_{eff} of the subsystem for the individual eigenstates across the energy spectrum is shown for some J_2 values (with $\delta = 0$).

study the effective Hilbert space dimension $(d_{\rm eff})$ of the subsystem for some representative points, (a) - (i), from Fig. 4. If ρ represents the reduced density matrix of the subsystem when the full system is in an eigenstate, then the effective Hilbert space dimension of the subsystem is defined as:

$$d_{\text{eff}} = \frac{1}{\text{Tr}(\rho^2)},\tag{4}$$

where Tr represents the trace operation over a basis of the subsystem. We note that this quantity can be considered as an entanglement measure and is related to the (quantum) Rényi entropy of order 2: $S_2(\rho) = -\log \text{Tr}(\rho^2) =$

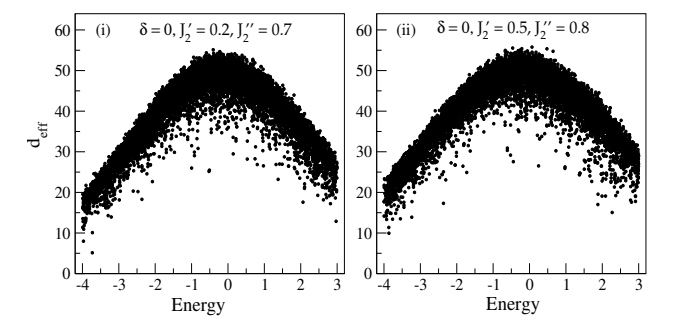


FIG. 8: Effective dimension d_{eff} profiles with broken SU(2) symmetry $(J_2' \neq J_2'')$.

 $\log(d_{\rm eff})$. For clarity, we note that when ρ is a pure state, the effective dimension $d_{\rm eff}=1$, while for a maximally mixed state, $d_{\rm eff}=D_1$, where D_1 denotes the Hilbert space dimension of the subsystem.

It is known that the average entanglement entropy (or equivalently, $d_{\rm eff}$) within a narrow energy window reaches its maximum possible value in systems that obey the ETH [44]. In such systems, the fluctuations of entropy around the average are also significantly suppressed. These results can be used to understand the thermalization behavior of our spin system. In the following, we first numerically study the individual effects of δ and J_2 on thermalization, subsequently, we investigate the thermalization properties of the spin model at selected points in the parameter space $\delta - J_2$. For the numerical calculations here, we take a system of size N=16 with a subsystem of size $N_s=6$.

To understand how dimerization (i.e., nonuniformity in the chain) affects thermalization, we first plot the effective dimension $d_{\rm eff}$ across the energy spectrum for various eigenstates at selected values of δ , keeping $J_2=0$. The resulting $d_{\rm eff}$ profiles are shown in Fig. 6. Likewise, to study the impact of the next-nearest-neighbor interactions, we plot $d_{\rm eff}$ for different values of J_2 with $\delta=0$; these results are presented in Fig.7. From these figures, we identify three characteristically different types of $d_{\rm eff}$ profiles:

- 1. A profile with high fluctuations in the values of d_{eff} without a clear branch structure, as seen for $(\delta = 0, J_2 = 0)$ in Fig. 6;
- 2. A multi-branched profile where distinct, narrow peaks appear at different energies with comparable prominence, as for $(\delta = 0.5, J_2 = 0)$ in the same figure;
- 3. A profile with broader, unequal branches, where a weaker structure appears beneath a more dominant one exemplified by the profile for $(\delta = 0, J_2 = 0.8)$ in Fig. 7.

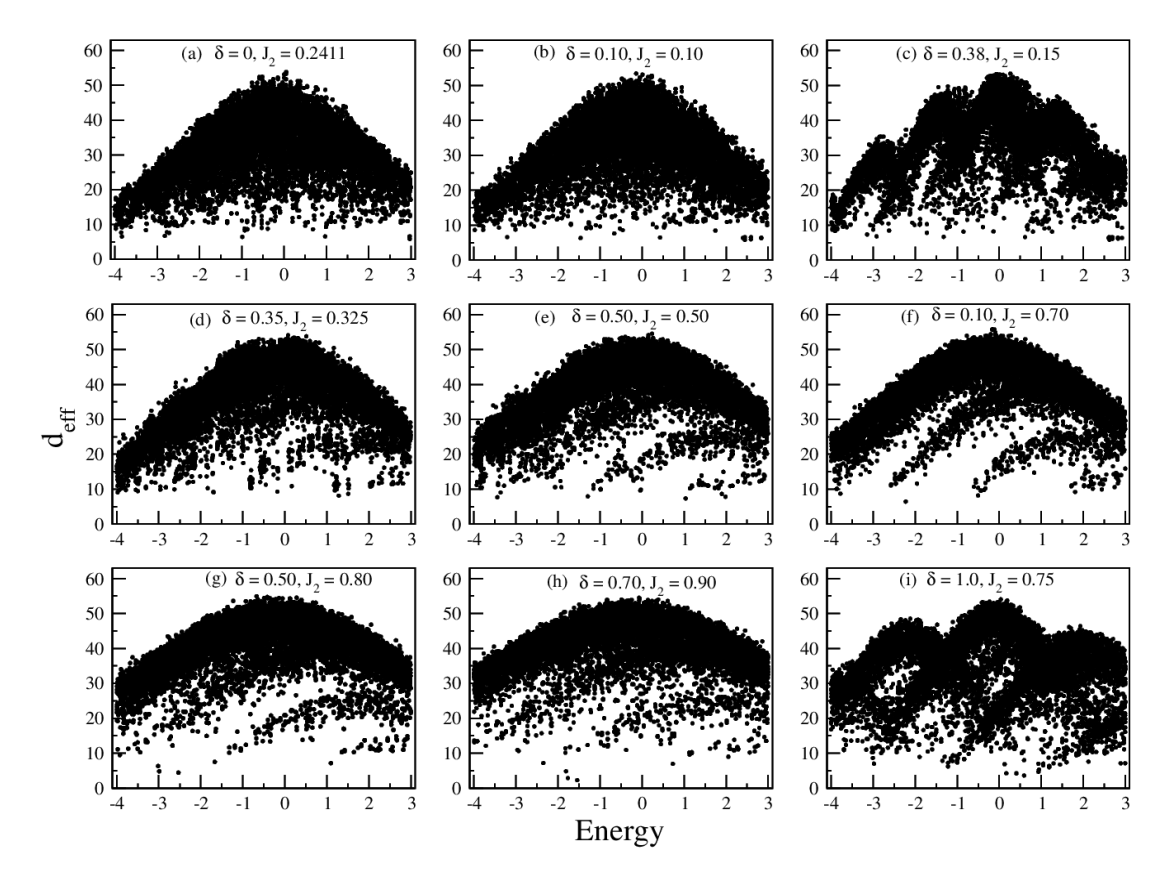


FIG. 9: Effective dimension d_{eff} of the subsystem for the individual eigenstates across the energy spectrum is shown for the nine selected points, (a) - (i), from Fig. 4.

The first type of profile corresponds to a violation of the ETH. The second type of profile results from the grouping of eigenvalues of the system (similar to what we have observed in the DOS profile for the point (j) in Fig. 3). The third type of profile is understood to be a consequence of the SU(2) symmetry in Hamiltonian of Eq. 1. Each branch in such profile corresponds to different total spin sectors, with the most prominent branch (the upper one) corresponds to the zero total spin.

To verify that the branches in the third type of d_{eff} profiles are due to the SU(2) symmetry, we take the same Hamiltonian with a symmetry breaking term:

$$H = J_1 \sum_{i=1}^{N} \left[1 + (-1)^i \delta \right] \mathbf{S}_i \cdot \mathbf{S}_{i+1}$$

$$+ J_2' \sum_{i=1}^{N} (S_i^x S_{i+2}^x + S_i^y S_{i+2}^y) + J_2'' \sum_{i=1}^{N} S_i^z S_{i+2}^z.$$
(5)

It may be noted that this Hamiltonian is the same as the one appears in Eq. 1, except that now we have different next-nearest-neighbor coupling strengths along the z and x (or y) spin components. The $d_{\rm eff}$ profiles, as appear in Fig. 8, do not now have branches that appear due to symmetry (as in Fig. 7). Since the original model under study has the SU(2) symmetry, it is expected that the

features of the third type of $d_{\rm eff}$ profile should also be present in the other two types of profiles. But we do not see this clearly since the fluctuations in the first type of profile are very high and the peaks are narrow in the second type of profile.

Having gained some insight into the effects of having finite δ and J_2 on thermalization, we now study the thermalization behavior of the dimerized $J_1 - J_2$ spin chain by analyzing the d_{eff} profiles at some selected points in the parameter space. The corresponding numerical results are shown in Fig. 9 (the calculations are done with a system size N = 16 and subsystem size $N_s = 6$). We make the following observations based on the results presented in this figure, and in the figures 6 and 7. When the system lies in the gapless ground-state phase $(0 \le J_2 \le J_{2c}, \delta = 0)$, the ETH is more prone to violation. This result is consistent with the earlier observation that the system thermalizes slowly for small J_2 without dimerization [45]. For larger J_2 values and weak dimerization (small δ), the ETH appears to be satisfied within each branch associated with a fixed total spin sector.

For $J_2 = 0$, the dimerization (δ) works as integrability breaking parameter. Without frustration, the system is integrable in the two limits: $\delta = 0$ and 1. For dimerization in between these two limits, the system is non-

Point	(δ,J_2)	\overline{S}_{vn}	σ_{sc}
a	(0.00, 0.2411)	3.59039	0.01698
b	(0.10, 0.10)	3.61727	0.01096 0.01794
c	(0.38, 0.15)	3.67362	0.01545
d	(0.35, 0.325)	3.71675	0.01266
e	(0.50, 0.50)	3.73651	0.01321
f	(0.10, 0.70)	3.74837	0.01600
g	(0.50, 0.80)	3.77011	0.01143
h	(0.70, 0.90)	3.76536	0.01422
i	(1.0, 0.75)	3.62846	0.02063

TABLE I: The average entropy (\overline{S}_{vn}) and the fluctuation in the expectation value of a local operator (σ_{sc}) are reported here for selected points, (a) - (i), from Fig. 4.

integrable [46]. It is interesting that for small δ and J_2 , although the system is nonintegrable, the thermal phase diagram (Fig. 4) shows that the fluctuation (σ_{sc}) in the expectation value of a local operator is reasonably large. Therefore, the system in this regime is expected to show slow thermalization, as observed earlier [46].

For intermediate to larger values of δ (with small J_2), the $d_{\rm eff}$ profile exhibits distinct branches, which arise due to the clustering of eigenvalues or modulations in the density of states (DOS). As mentioned earlier, for large δ (\sim 1) and small J_2 (< 0.5), the system is in a localized phase, hence the study of compliance of ETH is less meaningful here. For an intermediate value of δ (\sim 0.5) and a small value of J_2 (< 0.5), the system is expected to be ETH compliant, although not as strongly as in the regime where J_2 is large (> 0.5).

The results obtained here are overall consistent with what we have seen earlier by studying the expectation value of a local operator. We again see here that the ETH is not obeyed satisfactorily in the limits when both δ and J_2 are small (in the Néel phase), and the hypothesis holds better in the limits with intermediate δ values and intermediate to large values of J_2 (in the Spiral phase).

C. Average VN entropy

Let ρ_n be the reduced density matrix of the subsystem when the full system is in the eigenket $|n\rangle$. The corresponding von Neumann (VN) entropy of the subsystem is $S_{vn}(\rho_n) = -\text{Tr}(\rho_n \ln \rho_n)$. We define the average VN entropy over all eigenkets in the following way:

$$\overline{S}_{vn} = \frac{1}{D} \sum_{n=1}^{D} S_{vn}(\rho_n), \tag{6}$$

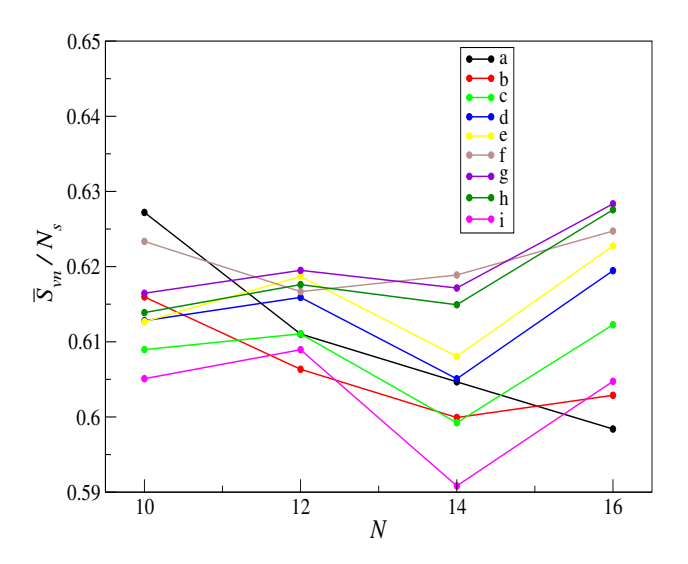


FIG. 10: The value of the ratio \overline{S}_{vn}/N_s for different system sizes N=8,10,12,14 and 16 at the selected points (δ,J_2) from Fig. 4.

where D is the total number of eigenkets (or the dimension of the Hilbert space of the full suystem). It is known that \overline{S}_{vn} follows a volume-law, i.e., this quantity is proportional to the size of the subsystem (in the leading term) [47–49]. The volume-law coefficient (or the proportionality constant) takes the maximum possible value for the nonintegrable (chaotic) systems, and is less than the maximum for the integrable systems. In general, we have the following expression for \overline{S}_{vn} :

$$\overline{S}_{vn} = \alpha_V N_s + \phi, \tag{7}$$

where ϕ is a function of both the system size N and the subsystem size N_s . It represents the non-universal subleading term, expected to be insignificant compared to the leading term when $1 < N_s \ll N$. For a nonintegrable system, in the $S_z = 0$ sector, the volume-law coefficient is expected to take a universal value: $\alpha_V = \ln(2) \approx 0.6931$.

For selected points in the parameter space $\delta - J_2$, we calculate this average entropy \overline{S}_{vn} to determine to what extent the ETH is satisfied. The numerical results are shown in Table I (the calculations are done with a system size N=16 and subsystem size $N_s=6$). We also show the corresponding values of σ_{sc} to check the consistency of the results. Both results in the table point out the overall same finding about thermalization: ETH holds stronger in the regime where δ takes intermediate values (~ 0.5) and the values of J_2 are between intermediate (~ 0.5) and large (~ 1).

D. Finite size scaling

To better assess whether the system is integrable or nonintegrable at a given point in the $\delta - J_2$ param-

eter space, one should examine how the relevant physical quantities scale with system size. A good quantity to study here is the ratio \overline{S}_{vn}/N_s . In the limit $N_s/N \to 0$, this ratio converges to α_V of Eq. 7. With increasing system size N (keeping N_s/N fixed at a small value), \overline{S}_{vn}/N_s is expected to increase and converge to $\alpha_V = \ln(2)$ if the system is nonintegrable (chaotic). On the other hand, the ratio should take a lower than the maximum value ($\alpha_V < \ln(2)$) for a large system size if the system is integrale.

In Fig. 10, we plot the ratio \overline{S}_{vn}/N_s as a function of the system size N for selected points in the parameter space. The calculations are done for the system sizes N=8,10,12,14 and 16 (the largest system size we could access) with corresponding subsystem sizes $N_s=2,3,4,5$ and 6. We choose the particular values of N_s so that the ratio N_s/N does not change much as we increase the system size. We see from the figure that, after some smaller values of N, the ratio \overline{S}_{vn}/N_s increases (especially from N=14 to 16) for all points except for the point associated with the gapless ground-state phase.

This finite-size scaling behavior reinforces our earlier observation: ETH is more likely to be violated by the system having a gapless ground-state phase, while it tends to hold for the system with the gapped ground-state phases. Moreover for finite but large system, ETH appears to be obeyed more robustly in the region where δ is of intermediate strength and J_2 takes moderate to

large values.

V. CONCLUSION

The thermalization property of the dimerized J_1-J_2 spin-1/2 model is investigated here. This model offers a minimal yet nontrivial setting to study thermalization under both inhomogeneity (via dimerization) and extended-range interactions (via next nearest-neighbor couplings). Our results suggest that the system is more likely to violate ETH when its ground-state phase is gapless ($0 \le J_2 \le J_{2c}$ with $\delta = 0$). Although the system is seen to obey ETH when its ground-state phases are gapped, a stronger compliance is expected in the region where δ is of intermediate strength and J_2 takes moderate to large values (the region is associated with the spiral ground-state phase of the model).

These findings demonstrate that controlled bond alternation provides a powerful tool for engineering thermalization in quantum simulators, with potential applications in quantum memory design. The results highlight how subtle modifications to interaction patterns can dramatically alter many-body dynamics, suggesting new pathways for controlling quantum thermalization in programmable quantum devices.

ACKNOWLEDGMENTS

SS thanks Ranjan Modak for useful discussions.

- J. M. Deutsch, Quantum statistical mechanics in a closed system, Phys. Rev. A 43, 2046 (1991).
- [2] M. Srednicki, Chaos and quantum thermalization, Phys. Rev. E 50, 888 (1994).
- [3] C. Gogolin and J. Eisert, Equilibration, thermalisation, and the emergence of statistical mechanics in closed quantum systems, Reports on Progress in Physics 79, 056001 (2016).
- [4] L. D'Alessio, Y. Kafri, A. Polkovnikov, and M. Rigol, From quantum chaos and eigenstate thermalization to statistical mechanics and thermodynamics, Advances in Physics 65, 239 (2016).
- [5] T. Mori, T. N. Ikeda, E. Kaminishi, and M. Ueda, Thermalization and prethermalization in isolated quantum systems: a theoretical overview, Journal of Physics B: Atomic, Molecular and Optical Physics 51, 112001 (2018).
- [6] V. Alba, Eigenstate thermalization hypothesis and integrability in quantum spin chains, Phys. Rev. B 91, 155123 (2015).
- [7] R. Steinigeweg, J. Herbrych, and P. Prelovšek, Eigenstate thermalization within isolated spin-chain systems, Phys. Rev. E 87, 012118 (2013).
- [8] J. M. Deutsch, Eigenstate thermalization hypothesis, Reports on Progress in Physics 81, 082001 (2018).
- [9] A. Dymarsky, N. Lashkari, and H. Liu, Subsystem eigen-

- state thermalization hypothesis, Phys. Rev. E **97**, 012140 (2018).
- [10] J. Šuntajs, J. Bonča, T. Prosen, and L. Vidmar, Ergodicity breaking transition in finite disordered spin chains, Phys. Rev. B 102, 064207 (2020).
- [11] S. Sugimoto, R. Hamazaki, and M. Ueda, Eigenstate thermalization in long-range interacting systems, Phys. Rev. Lett. 129, 030602 (2022).
- [12] H. Li, J. Wang, X.-J. Liu, and H. Hu, Many-body localization in ising models with random long-range interactions, Phys. Rev. A 94, 063625 (2016).
- [13] M. Rigol, V. Dunjko, V. Yurovsky, and M. Olshanii, Relaxation in a completely integrable many-body quantum system: An ab initio study of the dynamics of the highly excited states of 1d lattice hard-core bosons, Phys. Rev. Lett. 98, 050405 (2007).
- [14] A. C. Cassidy, C. W. Clark, and M. Rigol, Generalized thermalization in an integrable lattice system, Phys. Rev. Lett. 106, 140405 (2011).
- [15] D.-Z. Wang, H. Zhu, J. Cui, J. Argüello-Luengo, M. Lewenstein, G.-F. Zhang, P. Sierant, and S.-J. Ran, Eigenstate thermalization and its breakdown in quantum spin chains with inhomogeneous interactions, Phys. Rev. B 109, 045139 (2024).
- [16] D. Sels and A. Polkovnikov, Dynamical obstruction to localization in a disordered spin chain, Phys. Rev. E 104,

- 054105 (2021).
- [17] A. Pal and D. A. Huse, Many-body localization phase transition, Phys. Rev. B 82, 174411 (2010).
- [18] R. Nandkishore and D. A. Huse, Many-body localization and thermalization in quantum statistical mechanics, Annual Review of Condensed Matter Physics 6, 15 (2015).
- [19] M. Serbyn, Z. Papić, and D. A. Abanin, Quantum quenches in the many-body localized phase, Phys. Rev. B 90, 174302 (2014).
- [20] A. Chandran, A. Pal, C. R. Laumann, and A. Scardicchio, Many-body localization beyond eigenstates in all dimensions, Phys. Rev. B 94, 144203 (2016).
- [21] R. Mondaini and M. Rigol, Many-body localization and thermalization in disordered hubbard chains, Phys. Rev. A 92, 041601 (2015).
- [22] B. Lian, Quantum breakdown model: From many-body localization to chaos with scars, Phys. Rev. B 107, 115171 (2023).
- [23] J. Smith, A. Lee, P. Richerme, B. Neyenhuis, P. W. Hess, P. Hauke, M. Heyl, D. A. Huse, and C. Monroe, Many-body localization in a quantum simulator with programmable random disorder, Nature Physics 12, 907 (2016).
- [24] A. M. Kaufman, M. E. Tai, A. Lukin, M. Rispoli, R. Schittko, P. M. Preiss, and M. Greiner, Quantum thermalization through entanglement in an isolated manybody system, Science 353, 794 (2016).
- [25] P. Roushan, C. Neill, J. Tangpanitanon, V. M. Bastidas, A. Megrant, R. Barends, Y. Chen, Z. Chen, B. Chiaro, A. Dunsworth, A. Fowler, B. Foxen, M. Giustina, E. Jeffrey, J. Kelly, E. Lucero, J. Mutus, M. Neeley, C. Quintana, D. Sank, A. Vainsencher, J. Wenner, T. White, H. Neven, D. G. Angelakis, and J. Martinis, Spectroscopic signatures of localization with interacting photons in superconducting qubits, Science 358, 1175 (2017).
- [26] W. Beugeling, R. Moessner, and M. Haque, Finite-size scaling of eigenstate thermalization, Phys. Rev. E 89, 042112 (2014).
- [27] J. D. Noh, Eigenstate thermalization hypothesis and eigenstate-to-eigenstate fluctuations, Phys. Rev. E 103, 012129 (2021).
- [28] N. Laflorencie, Quantum entanglement in condensed matter systems, Physics Reports 646, 1 (2016).
- [29] M. Foss-Feig, P. Niroula, J. T. Young, M. Hafezi, A. V. Gorshkov, R. M. Wilson, and M. F. Maghrebi, Emergent equilibrium in many-body optical bistability, Phys. Rev. A 95, 043826 (2017).
- [30] M. Pino, Entanglement growth in many-body localized systems with long-range interactions, Phys. Rev. B 90, 174204 (2014).
- [31] B. Neyenhuis, J. Zhang, P. W. Hess, J. Smith, A. C. Lee, P. Richerme, Z.-X. Gong, A. V. Gorshkov, and C. Monroe, Observation of prethermalization in long-range interacting spin chains, Science Advances 3, e1700672 (2017).
- [32] J. T. Schneider, J. Despres, S. J. Thomson, L. Tagliacozzo, and L. Sanchez-Palencia, Spreading of correlations and entanglement in the long-range transverse ising chain, Phys. Rev. Res. 3, L012022 (2021).
- [33] N. Ranabhat and M. Collura, Thermalization of long

- range ising model in different dynamical regimes: A full counting statistics approach, SciPost Phys. Core **7**, 017 (2024).
- [34] J. A. Kjäll, J. H. Bardarson, and F. Pollmann, Manybody localization in a disordered quantum ising chain, Phys. Rev. Lett. 113, 107204 (2014).
- [35] R. Chitra, S. Pati, H. R. Krishnamurthy, D. Sen, and S. Ramasesha, Density-matrix renormalization-group studies of the spin-1/2 heisenberg system with dimerization and frustration, Phys. Rev. B 52, 6581 (1995).
- [36] C. K. Majumdar and D. K. Ghosh, On next-nearestneighbor interaction in linear chain. i, Journal of Mathematical Physics 10, 1388 (1969).
- [37] K. Okamoto and K. Nomura, Fluid-dimer critical point in s = 1/2 antiferromagnetic heisenberg chain with next nearest neighbor interactions, Physics Letters A 169, 433 (1992).
- [38] U. Schollwöck, The density-matrix renormalization group in the age of matrix product states, Annals of Physics 326, 96 (2011).
- [39] B. S. Shastry, Exact solution of an s=1/2 heisenberg antiferromagnetic chain with long-ranged interactions, Phys. Rev. Lett. 60, 639 (1988).
- [40] D. P. Goli, S. Sahoo, S. Ramasesha, and D. Sen, Quantum phases of dimerized and frustrated heisenberg spin chains with s=1/2, 1 and 3/2: an entanglement entropy and fidelity study, Journal of Physics: Condensed Matter **25**, 125603 (2013).
- [41] F. D. M. Haldane, Nonlinear field theory of large-spin heisenberg antiferromagnets: Semiclassically quantized solitons of the one-dimensional easy-axis néel state, Phys. Rev. Lett. 50, 1153 (1983).
- [42] S. Sahoo, R. Rajamani, S. Ramasesha, and D. Sen, Fully symmetrized valence-bond based technique for solving exchange hamiltonians of molecular magnets, Phys. Rev. B 78, 054408 (2008).
- [43] S. Sahoo and S. Ramasesha, Full spin and spatial symmetry adapted technique for correlated electronic hamiltonians: Application to an icosahedral cluster, International Journal of Quantum Chemistry 112, 1041 (2012).
- [44] S. Mishra and S. Sahoo, Quantum thermalization and average entropy of a subsystem, arXiv 10.48550/arXiv.2506.19896 (2025).
- [45] N. P. Konstantinidis, Thermalization away from integrability and the role of operator off-diagonal elements, Phys. Rev. E 91, 052111 (2015).
- [46] N. P. Konstantinidis, Thermalization of a dimerized antiferromagnetic spin chain, J. of Phys.: Condens. Matter 28, 026001 (2015).
- [47] T. LeBlond, K. Mallayya, L. Vidmar, and M. Rigol, Entanglement and matrix elements of observables in interacting integrable systems, Phys. Rev. E 100, 062134 (2019).
- [48] E. Bianchi, L. Hackl, M. Kieburg, M. Rigol, and L. Vidmar, Volume-law entanglement entropy of typical pure quantum states, PRX Quantum 3, 030201 (2022).
- [49] L. Vidmar, L. Hackl, E. Bianchi, and M. Rigol, Entanglement entropy of eigenstates of quadratic fermionic hamiltonians, Phys. Rev. Lett. 119, 020601 (2017).